J Comput Aided Mol Des (2011) 25:213–222
DOI 10.1007/s10822-011-9412-6

Structure–activity relationships of diphenyl-ether as protoporphyrinogen oxidase inhibitors: insights from computational simulations

Ge-Fei Hao · Ying Tan · Ning-Xi Yu · Guang-Fu Yang

Received: 10 July 2010 / Accepted: 10 January 2011 / Published online: 23 January 2011

Abstract Protoporphyrinogen oxidase (PPO, EC 1.3.3.4), which has been identified as a significant target for a great family of herbicides with diverse chemical structures, is the last common enzyme responsible for the seventh step in the biosynthetic pathway to heme and chlorophyll. Among the existing PPO inhibitors, diphenyl-ether is the first commercial family of PPO inhibitors and used as agriculture herbicides for decades. Most importantly, diphenyl-ether inhibitors have been found recently to possess the potential in Photodynamic therapy (PDT) to treat cancer. Herein, molecular dynamics simulations, approximate free energy calculations and hydrogen bond energy calculations were integrated together to uncover the structure–activity relationships of this type of PPO inhibitors. The calculated binding free energies are correlated very well with the values derived from the experimental k_i data. According to the established computational models and the results of approximate free energy calculation, the substitution effects at different position were rationalized from the view of binding free energy. Some outlier (*e.g.* LS) in traditional QSAR study can also be explained reasonably. In addition, the hydrogen bond energy calculation and interaction analysis results indicated that the carbonyl oxygen on position-9 and the NO_2 group at position-8 are both vital for the electrostatic interaction with Arg98, which made a great contribution to the binding free energy. These insights from computational simulations are not only helpful for understanding the molecular mechanism of PPO-inhibitor interactions, but also beneficial to the future rational design of novel promising PPO inhibitors.

Keywords Protoporphyrinogen oxidase · Diphenyl-ether inhibitor · Molecular dynamics simulations · Structure–activity relationship

Abbreviations

PPO	Protoporphyrinogen oxidase
PDT	Photodynamic therapy
SAR	Structure activity relationship
AF	Acifluorfen
AFM	Acifluorfen-methyl
HBE	Hydrogen bond energy

Introduction

Protoporphyrinogen oxidase (PPO, EC 1.3.3.4) is the last common enzyme catalyzing the seventh step in the biosynthetic pathway leading to heme and chlorophyll [1–3]. It exists in both chloroplast and mitochondria of the plant, which were called PPO1 and PPO2, respectively [4, 5]. PPO can remove hydrogen atoms from protoporphyrinogen IX to form protoporphyrin IX which seems to be ubiquitous in cells having aerobic metabolism [6, 7]. Inhibition of this enzyme will lead to the accumulation of protoporphyrinogen IX, which will be slowly oxidized to protoporphyrin IX by O_2 in the mitochondrion and chloroplast [8]. This spontaneous process will result in serious consequences: In

Electronic supplementary material The online version of this article (doi:10.1007/s10822-011-9412-6) contains supplementary material, which is available to authorized users.

G.-F. Hao · Y. Tan · N.-X. Yu · G.-F. Yang (✉)
Key Laboratory of Pesticide & Chemical Biology of Ministry of Education, College of Chemistry, Central China Normal University, 152 Luoyu Road, Wuhan 430079, Hubei, People's Republic of China
e-mail: gfyang@mail.ccnu.edu.cn

the presence of light, the photosensitive protoporphyrin IX will induce the generation of singlet oxygen that causes lipid peroxidation and cell death [9–11]. In the field of agrochemicals, this enzyme has been identified as a significant target for a great family of herbicides with diverse chemical structures, including diphenylethers, phenylpyrazoles, oxadiazoles, triazolinones, thiadiazoles, pyrimidindiones, oxazolidinedione, and N-phenyl-phthalimides [12–14].

Diphenyl-ether is the first group of commercial herbicides targeting PPO, among which nitrofen is the first product entered market in the early 1960s [15]. These herbicides are called contact and light-depended herbicides and used to control certain annual broadleaf and grassy weeds in vegetables, fruit, cotton, ornamentals and rice [14, 16, 17]. Except for its application in the agrochemical areas, the most potential application of diphenyl-ether inhibitors is a treatment of cancer through photodynamic therapy (PDT) [18, 19], which is also potentially valuable in sterilization [20]. For example, it is being investigated for treatment of psoriasis [21], and an approved treatment for wet macular degeneration [22]. PDT matured as a feasible medical technology in the 1980s at several institutions throughout the world involving three key components: a photosensitizer, light, and tissue oxygen [23, 24]. If photosensitizers are established in high concentrations in the tumor cells and these tumors are exposed to irradiation with light of an appropriate wavelength, the photosensitizer will be activated and tumor cells will be destroyed [25]. Protoporphyrin IX is an extremely effective natural photosensitizer, but it cannot take effect before activation. Halling et al. [26] has showed that PPO inhibitors could activate protoporphyrin IX and cause its accumulation within tumor cells. The diphenyl-ether inhibitors was foremost found to have good bioactivity to human PPO and have potential ability to be an activator for protoporphyrin IX [27, 28].

Structure–activity relationship (SAR) studies on diphenyl-ether herbicides have been extensively reported [29–31]. Previous QSARs performed at two or multi-dimensional level reproduced the activity of individual data sets relatively well. However, these models based on the conformation and physicochemical properties of inhibitors could not be used to predict the activity of structurally influenced derivatives, if one is interested in understanding the relationship between structural characteristics of inhibitors and their binding site. By far three crystal structures of PPO from tobacco, *Myxococcus xanthus*, and *Bacillus subtilis* were resolved [32–34], but it is a pity that the sequence similarities between human PPO and the three structures are no more than 30% which bring difficulty for homology modeling of human PPO [35, 36]. Fortunately, reports of the crystal structures of PPO show that PPOs from different families have very similar structures and conservative binding envelope [32, 33]. It is especially surprising that diphenyl ether inhibitors have comparatively bioactivity for different PPO families [37]. Therefore, tobacco PPO2 is an undoubtly useful model system for the understanding of structure–activity relationships between diphenyl ether inhibitors and human PPO.

In the present study, to clarify the structure–activity relationships of diphenyl-ether inhibitors, we carried out molecular dynamics simulations of PPO in complex with four diphenyl ether inhibitors including acifluorfen (AF), acifluorfen-methyl (AFM), LS, and RH, (shown in Scheme 1) and binding free energy analysis as well as free energy decomposition. Our simulations results indicated that the calculated binding free energies were in good agreement with available experimental data, suggesting that the computational protocol used in this study may be useful for rational design of new PPO inhibitors in the future.

Computational methods

Molecular dynamics simulations

Before the molecular dynamics (MD) simulations, the geometries of ligands were optimized by performing first-principles electronic potential calculations at the HF/6-31 + G* level using the Gaussian03 program [38]. The ESP partial atom charges were determined using the Merz–Singh–Kollman scheme [39, 40]. On the basis of the calculated electrostatic potential, Antechamber module of the Amber8 program [41] was used to produce the RESP charges required for the MD simulations.

The starting structure of the MD simulations used in the present study were constructed based on the X-ray crystal structures of tobacco PPO complexed with INH and *Myxococcus xanthus* PPO complexed with AF (PDB code: 1SEZ and 2IVD, respectively). The missing atoms were added and two crystal structures were aligned with the AF placed into the active site of tobacco PPO. The other three complexes of inhibitors: AFM, LS, and RH were acquired

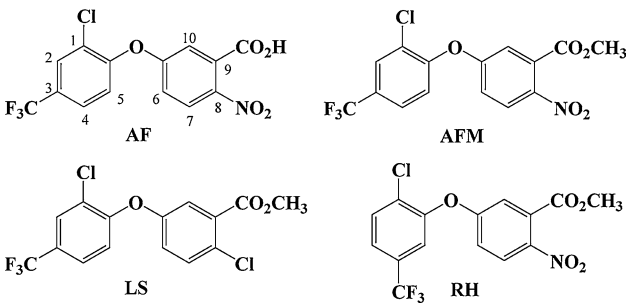

Scheme 1 Chemical structures of diphenyl ether PPO inhibitors

by directly modifying on the complex structure of tobacco PPO and AF. All of the above works were completed by using the software sybyl7.1 [42].

To carry out the MD simulations, the topologic and coordinate files of the four complexes were built with Leap module of the Amber8 package. All the minimizations and MD simulations were performed with Sander module of Amber8. The AMBER ff99 force field [43] was used as the parameters for amino acid residues and the general AMBER force field (gaff) [44] was used as the parameters for ligands. To ensure overall electroneutrality of the system, appropriate number of counter ions Na^+ ions was added to the most electronegative areas around the protein. The entire protein was subsequently solvated in a box of TIP3P water molecules with a margin of 10.0 Å in each direction from the solute [45]. The particle mesh Ewald (PME) [46, 47] was applied to calculate long-range electrostatic interactions. The cutoff distance for the long-range electrostatic and the *van der Waals* (vdW) energy terms was set at 10.0 Å. SHAKE algorithm was used to constrain all covalent bonds involving hydrogen atoms [48]. To avoid edge effects, the periodic boundary conditions were applied in MD simulation.

A three-step minimization procedure was performed. First, movement was allowed only for the solvent and ion molecules with a harmonic constraints (500 kcal/mol $Å^2$) applied to the complex. Second, the mainchain atoms of the protein were fixed with the same strength as the above and other atoms were allowed to move. Finally, all atoms were minimized with no restraint. In each step, energy minimization was first executed for 2,000 steps by the steepest descent method and the conjugated gradient method for the subsequent 3,000 steps. Afterward, MD simulations were performed as followings: First, the solvent molecules were heated for 10 ps to ensure that the protein was sufficiently enclosed by waters. Then system was gradually heated from 10 to 300 K over 20 ps and equilibrated in 180 ps with the coordinates of inhibitor and its surrounding residues (less than 6 Å) being constrained. Finally the whole complex was relaxed for a 2.5 ns equilibrating calculation executed at 1 atm and 300 K. The time step used for the MD simulations was set to 2.0 fs. During the MD simulation process, coordinates were collected every 1 ps.

Binding free energy analysis

The predictions of free energies of complex, receptor, and inhibitor were based on snapshots taken from a single trajectory of the complex MD simulation. At first, a total of 100 snapshots were taken from the last 1 ns trajectory with an interval of 10 ps and the counterions and water molecules were stripped. MM-PBSA approach implemented in the Amber8 program was applied to compute the binding free energy difference between the free energies of the protein–ligand complex (G_{cpx}) and the unbound protein (G_{rec}) and ligand (G_{lig}). The introduction of MM-PBSA method had been described before [49]. Generally, the protein–ligand approximate free energy was calculated by using the equations below:

$$\Delta G_{bind} = G_{cpx} - (G_{rec} + G_{lig}) \quad (1)$$

In which, the ΔG_{bind} is evaluated as follows:

$$\Delta G_{bind} = \Delta E_{MM} + \Delta G_{sol} - T\Delta S \quad (2)$$

ΔG_{bind} was considered as a sum of the changes in the molecular mechanical (MM) gas-phase binding energy (ΔE_{MM}), solvation energy (ΔG_{sol}), and entropy term ($-T\Delta S$). The ΔE_{MM} is calculated by Eq. 3, where ΔE_{val}, ΔE_{ele} and ΔE_{vdw} represent the internal energy contribution from bonds, angles and torsions, electrostatic and van der Waals interactions, respectively, which are computed using the same parameter set as that used in the MD simulation.

$$\Delta E_{MM} = \Delta E_{val} + \Delta E_{ele} + \Delta E_{vdw} \quad (3)$$

$$\Delta G_{sol} = \Delta G_{PB} + \Delta G_{np} \quad (4)$$

The solvation free energy ΔG_{sol} consists of two parts. The electrostatic contribution to the solvation free energy (ΔG_{PB}) is calculated by Poisson-Boltzmann (PB) method using the Delphi program [50]. The grid spacing was set to 1/2 Å. The values of the dielectric constant for protein and water were respectively set to 1 and 80. The atomic charges of the protein were taken from the ff99 force field. The nonpolar solvation contribution (ΔG_{np}) is estimated as follows:

$$\Delta G_{np} = \gamma SASA + \beta \quad (5)$$

where SASA is the solvent-accessible surface area and the solvation parameters, γ is set to 0.00542 kcal/mol $Å^2$ and β is set to 0.92 kcal/mol [51]. The probe radius of the solvent is 1.4 Å. The atomic radii of the solute were taken from the PARSE parameter set [50].

The normal-mode analysis was performed to estimate the conformational entropy change upon ligand binding using the nmode program in Amber8 [52]. Each snapshot was fully minimized to an convergence criterion of 1 x 10^{-4} kcal mol^{-1} $Å^{-1}$. Owing to the high computational cost, only residues around the inhibitor (less than 8 Å) were retained to estimate the contribution of the entropies, which was the same as the strategy that we applied before [53]. To theoretically evaluate the reliability of the calculated ΔG values, the standard error (SE) of the calculated free energy was estimated by using Eq. 6, which is related to both the number (N) of snapshots chosen for the calculations and the root-mean-square fluctuation (RMSF) of the calculated ΔG values associated with all snapshots [54]:

$$SE = RMSF/\sqrt{N} \quad (6)$$

Hydrogen bond analysis

In this work, the Ptraj module of Amber8 program was used to do the hydrogen bond analysis. To better understand the overall strength of hydrogen bonding between the ligand and protein, the hydrogen bond energy (HBE) was calculated using the empirical HBE equation implemented in the Autodock3.05 program [55]. The general HBE equation is $HBE(r) \approx 5\varepsilon r_{eqm}^{12}/r^{12} - 6\varepsilon r_{eqm}^{10}/r^{10}$, in which r is the distance between hydrogen atom (H) and hydrogen bond acceptor (A), r_{eqm} is the equilibrium internuclear distance between H and A, and ε is the energy well depth at r_{eqm}. The HBE was evaluated as the average value of each snapshot taken from the last 1 ns, which has been discribed in our previous work [53].

Results and discussion

Validation of the MD model

Firstly, the obtained MD-simulated binding mode was compared with the reported crystal structure of *Myxococcus xanthus* PPO in complex with AF [33, 56]. As shown in Fig. 1, the substituted phenyl ring B was sandwiched between two conserved residues of Leu372 and Leu356 (allele to *Myxococcus xanthus* Ile345 and Leu332, respectively), while the phenyl ring A was sandwiched between the residues of Phe392 and Gly175 (allele to *Myxococcus xanthus* Met365 and Gly167, respectively). In addition, Arg98 (allele to *Myxococcus xanthus* Arg95) formed hydrogen bonds with AF.

Secondly, plots of the root-mean-square deviation (d_{RMS}) of the protein backbone atoms and ligand along the entire process of the MD simulation were shown to investigate the convergence and equilibration of the simulation. As shown in Fig. 2, after 1,700 ps the d_{RMS} of the protein backbone atoms stabilized around 2 Å for 1 ns. To further validate the equilibrium, the distances of the hydrogen bonds between Arg98 and inhibitors during the MD simulations were monitored (Fig. 3). It is found that these key distances were stabilized during the equilibration process of the MD simulation. Therefore, the subsequent binding free energy analyses in each case were based on the MD trajectory truncated between 2.7 and 3.7 ns.

Finally, to further approve the reliability of the simulation, the calculated binding affinities of the four inhibitors were compared with the available experimental data. The results included the overall binding free energy and all of the energy terms for each compound (shown in Table 1). As listed in Table 1, the binding free energies (ΔG_{cal}) obtained from the MM–PBSA calculations are −8.65, −12.99, −11.34, and −9.16 kcal/mol, which are in good agreement with the experimentally-derived binding free energies (ΔG_{exp}), −9.69, −12.43, −11.47, and −9.97 kcal/mol for the PPO binding with AF, AFM, LS, and RH respectively. The qualitative order of the calculated binding affinities of the inhibitors is AFM > LS > RH > AF (from the highest binding affinity to the lowest), which is in accordance with the experimental order. Quantitatively, the average absolute deviation between the calculated binding free energies and the corresponding experimental values is 0.64 kcal/mol. The good agreement between the computational results and the experimental data suggests that the computational models constructed and tested in this study should be reliable.

Analysis of the interaction between PPO and ligands

According to the experimental data, AFM has the strongest binding affinity. As can be found in Table 1, the energy component analysis shows that the sum of the *van der Waals* interaction (−51.68 kcal/mol) and the electrostatic interaction (−24.74 kcal/mol) between AFM and PPO are

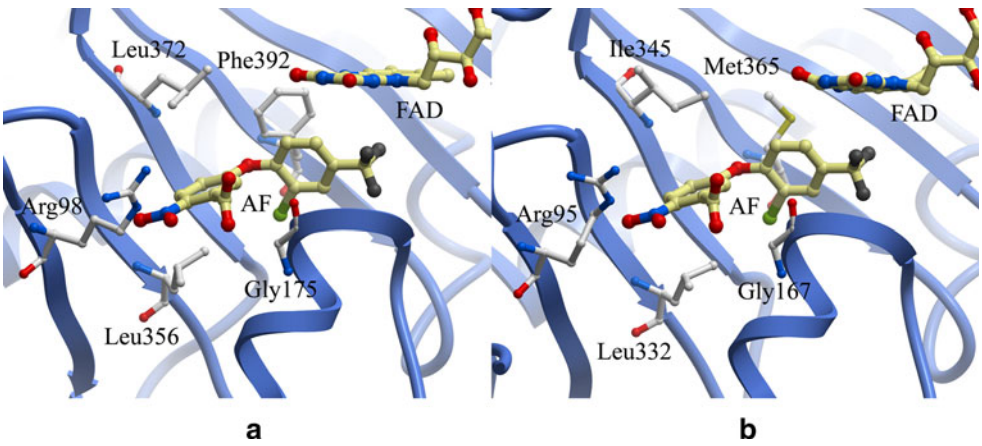

Fig. 1 Comparison of the simulated model with the crystal structures of *M. Xanthus* PPO in complex with AF. **a** The simulated binding mode of tobacco PPO in complex with AF. **b** The crystal structure of *M. Xanthus* PPO in complex with AF

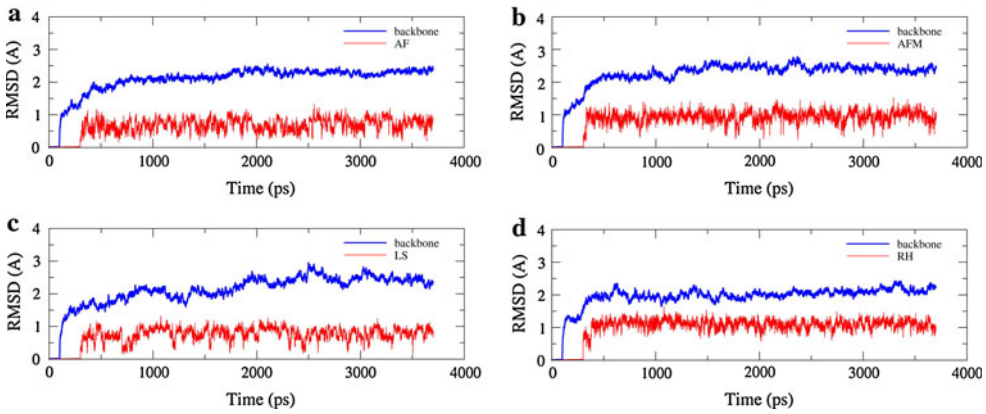

Fig. 2 Time dependence of the RMSD of protein backbone atoms (*color in blue*) and inhibitors (*color in red*). **a** PPO-AF, **b** PPO-AFM, **c** PPO-LS, and **d** PPO-RH

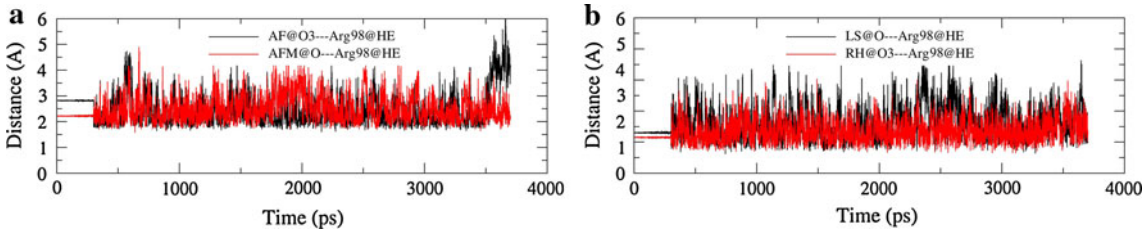

Fig. 3 The distance of hydrogen bond between Arg98 and inhibitors. **a** AF and AFM. **b** LS and RH

stronger than those between AF and PPO (−49.00 and −20.69 kcal/mol), LS and PPO (−49.26 and −13.32 kcal/mol), RH and PPO (−51.08 and −23.44 kcal/mol). However, because of the high cost of the free energy of solvation, the binding of AFM (−25.54 kcal/mol) is statistically no difference with that of AF (−25.58 kcal/mol) and is only slightly stronger than that of LS (−24.41 kcal/mol) and RH (−24.85 kcal/mol). Here, it must be specially emphasized that the interaction energy in gas between LS and PPO is largely reduced to −62.58 kcal/mol in comparison with that (−76.42 kcal/mol) between AFM and PPO, but the binding energy of LS with PPO (−24.41 kcal/mol) was only slightly reduced. One important reason is that it has the lowest expense in the solvation free energy because of the less change (140.8 $Å^2$) in the polar surface area (PSA) of receptor upon LS binding (shown in Table 1), which was calculated based on the averaged structure of 100 snapshots by using the insightII [57].

The calculated conformational entropic contributions ($-T\Delta S$) for each inhibitor binding with PPO are largely different, with values ranging from 12.55 to 16.93 kcal/mol. The conformational entropy can be divided into three parts: transitional, rotational, and vibrational entropy change according to partition function. We noticed that the large difference in the entropy change come from the vibrational entropy change which did favorable contributions to the inhibitor binding depicted in the Table 1 and it was because of the change of the flexibility of the complex structure. During the ligand-binding process, the vibrational entropy of the complex decreases with the binding of the ligand. For a ligand with a better "induced-fit" effect to the protein, there may be a smaller vibrational entropy lost between unbind and binding states, which lies on the flexibility of the complex. And this has been clearly explained in a recently published paper [58]. The inhibitors: AFM and LS had smaller binding envelopes (3,528 and 3,952 $Å^3$ respectively) than that of AF and RH (4,506 and 4,222 $Å^3$ respectively), which indicated that AFM and LS possess more appropriate and compact binding with the active envelope than AF and RH. Because smaller volume may mean a better "induced-fit" effect, and the conformational change of the complex is always driven by the generation of the ligand force, which has also been proved elsewhere [58].

In order to gain a detailed picture of protein-inhibitor interactions and the contribution of each residue, the binding energy in four complexes was decomposed on per residue located within 6 Å of the ligand by using Anal module of Amber8 program (shown in Table 2 and Fig. 4). The quantitative information is significant to the understanding of binding mechanism for inhibitors. As can be seen from Table 2 and Fig. 4, the residues with most favorable contributions (almost larger than 3.0 kcal/mol) to the binding free energy in all of these systems are Arg98, Phe170, Gly175, Phe353, Val355, Leu356, Leu372, Phe392, and coenzyme FAD. Generally, the interaction spectrums of the four inhibitors are quite similar. As far as we can see that most of the above residues are nonpolar, so the more hydrophobic the binding pocket and the ligand

Table 1 Binding free energies (kcal/mol) of AF, AFM, LS, and RH

Ligand	ΔE_{ELE}	ΔE_{VDW}	ΔE^{a}_{GAS}	ΔG_{SOL}	ΔPSA^{b} (Å^2)	ΔG_{PB}	$-T\Delta S$	$-T\Delta S$ (Vib)	Vol (Å^3)	ΔG^{c}_{cal}	ΔG^{d}_{exp}
AF	−20.69 (0.32)[e]	−49.00 (0.22)	−69.69 (0.37)	44.12 (0.40)	237.20	−25.58 (0.31)	16.93 (0.65)	−6.71 (0.65)	4,506	−8.65	−9.69
AFM	−24.74 (0.31)	−51.68 (0.25)	−76.42 (0.38)	50.88 (0.42)	234.40	−25.54 (0.37)	12.55 (0.80)	−11.17 (0.80)	3,528	−12.99	−12.43
LS	−13.32 (0.27)	−49.26 (0.24)	−62.58 (0.37)	38.17 (0.39)	140.80	−24.41 (0.33)	13.07 (0.78)	−10.58 (0.77)	3,952	−11.34	−11.47
RH	−23.44 (0.28)	−51.08 (0.24)	−74.52 (0.36)	49.66 (0.41)	216.20	−24.85 (0.31)	15.69 (0.73)	−8.04 (0.72)	4,222	−9.16	−9.97

[a] The interaction in gas phase: $\Delta E_{GAS} = \Delta E_{ELE} + \Delta E_{VDW}$

[b] The change of polar surface area (ΔPSA) is calculated by using $\Delta PSA = PSA_{rec} + PSA_{lig} - PSA_{cpx}$

[c] The results determined by the MM-PBSA calculations

[d] The experimental values ΔG_{exp} were derived from the reported experimental k_i values of maize PPO which is highly homologous protein of tobacco PPO [37]

[e] The values in parentheses are standard error (SE)

are, the more contributive the solvation effect of the complex is to the binding free energy. Meanwhile, the electrostatic interaction (hydrogen bonds) between Arg98 and inhibitor also has an important role for the inhibitor binding which also match the pre-QSAR study that an electrostatic component around the position-9 (see Scheme 1) can increase the binding affinity [59].

To analyze conformational changes of the binding pocket, the average structures of the four receptor-ligand complexes from the equilibration stage (last 1 ns) of the MD simulation were obtained by averaging 1,000 snapshots. For convenient, AFM was set as a reference for the other three complexes due to its highest binding affinity. Fig. 5 shows the superposition of the binding site of AFM structure with the other structures. Fig. 5 obviously indicated that, except that the side chain of Phe172 rotated about 75 degree, the binding pockets of AF and RH took very similar conformation to that of AFM. On the contrary, the binding pocket of LS suffered from significant conformational change, the side chain of Phe353 rotated about 115 degree.

AF displayed lower activity than AFM because the ester group in AFM was replaced with smaller acid group in AF. From Table 1 we can conclude that this substitution resulted in the reduction of electrostatic and *van der Waals* interaction energies. Fortunately, this energy lost was compensated in part by solvation energy. But unfortunately, a large cost of entropy change was found for AF. As a consequence, AF has unfavorable binding free energy to AFM. This result is in good agreement with the 3D-QSAR study that a bulky substituent at the position-9 are favorable for the PPO-inhibition activity [59].

Compared with that of AFM, most residues of the binding pocket of LS took significant conformational changes, such as the side chain of residues Arg98, Phe172, Phe353, Leu372, and Phe392. The NO_2 group of AFM formed electrostatic interactions with Arg98. However, this NO_2 group was replaced by Cl atom in LS. As a consequence, the interaction of LS with Arg98 reduced greatly from about 16.92 to 9.49 kcal/mol (Table 2 and Fig. 4). However, LS still displayed the same level of PPO inhibition activity as AFM. From the results as shown in Table 1, we can conclude that the lost electrostatic interaction was partly compensated by the solvation free energy because the chlorine atom improved the hydrophobic property of LS. In addition, the entropy change also partly compensated the enthalpy change (see Table 1). Because most traditional 3D-QSAR study cannot taken solvation and entropy effects into account, compound LS is an outlier in QSAR study [60].

Furthermore, except for the rotation of the side chain of Phe172, the movement of Phe392 and Leu372 were also found in the model of RH. As shown in scheme 1, the CF_3

Table 2 Interaction energies between the PPO residues and each ligand

PPO Residue[a]	Ligand-residue interaction energy (kcal/mol)			
	AF	AFM	LS	RH
Ala66	0.27 (0.01)[b]	0.25 (0.01)	0.13 (0.00)	−0.04 (0.01)
Asn67	0.43 (0.02)	0.46 (0.01)	−1.40 (0.07)	0.18 (0.02)
Thr68	−0.48 (0.02)	−0.84 (0.04)	−0.27 (0.02)	−0.38 (0.02)
Arg98	**−15.00 (0.28)**	**−16.92 (0.24)**	**−9.49 (0.23)**	**−17.58 (0.22)**
Tyr99	−0.12 (0.03)	0.04 (0.03)	−0.13 (0.01)	0.08 (0.02)
Pro169	−0.71 (0.01)	−0.94 (0.02)	−0.55 (0.01)	−1.14 (0.02)
Phe170	**−1.39 (0.06)**	**−3.49 (0.13)**	**−3.23 (0.11)**	**−4.50 (0.11)**
Phe172	−2.83 (0.04)	−2.90 (0.05)	−2.39 (0.03)	−3.08 (0.06)
Gly175	**−5.23 (0.07)**	**−5.98 (0.08)**	**−5.46 (0.07)**	**−5.96 (0.09)**
Thr174	−2.15 (0.05)	−3.16 (0.07)	−2.82 (0.07)	−2.55 (0.07)
Cys175	−1.30 (0.03)	−1.26 (0.05)	−1.40 (0.03)	−0.76 (0.04)
Gly176	−0.21 (0.02)	−0.23 (0.02)	−0.25 (0.02)	0.05 (0.02)
Leu334	−0.77 (0.05)	−0.76 (0.04)	−1.04 (0.06)	−1.07 (0.05)
Phe353	**−3.95 (0.07)**	**−4.04 (0.05)**	**−2.78 (0.05)**	**−4.28 (0.06)**
Gly354	1.71 (0.10)	1.61 (0.09)	0.30 (0.03)	0.53 (0.10)
Val355	**−3.99 (0.07)**	**−3.33 (0.07)**	**−2.66 (0.04)**	**−2.53 (0.08)**
Leu356	**−4.95 (0.07)**	**−4.89 (0.07)**	**−4.48 (0.08)**	**−4.03 (0.08)**
Leu369	−1.46 (0.03)	−1.48 (0.03)	−1.76 (0.04)	−1.50 (0.04)
Gly370	−0.63 (0.04)	−0.87 (0.03)	−0.67 (0.03)	−1.43 (0.04)
Thr371	−1.81 (0.06)	−2.37 (0.06)	−2.47 (0.05)	−2.07 (0.05)
Leu372	**−4.68 (0.07)**	**−4.47 (0.07)**	**−3.55 (0.07)**	**−4.02 (0.07)**
Phe392	**−5.73 (0.06)**	**−5.68 (0.06)**	**−5.34 (0.06)**	**−5.94 (0.08)**
Ala438	−0.12 (0.00)	−0.14 (0.00)	−0.14 (0.01)	0.03 (0.01)
Phe439	−0.96 (0.03)	−0.82 (0.03)	−1.08 (0.02)	−0.91 (0.02)
FAD	**−7.87 (0.11)**	**−7.73 (0.12)**	**−4.18 (0.09)**	**−3.50 (0.06)**

Bold residues show the most favorable interactions (where nearly all the ligands showed energies larger than 3.0 kcal/mol)

[a] The residues were located within 6 Å of the ligand

[b] The values in parentheses are standard errors (SE)

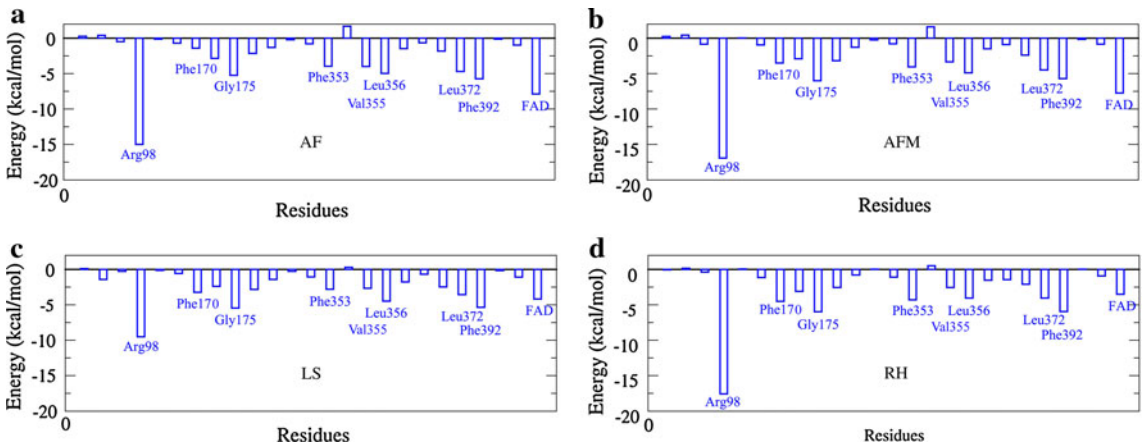

Fig. 4 Inhibitor-residue interaction spectrum of **a** AF-PPO complex, **b** AFM-PPO complex, **c** LS-PPO complex, and **d** RH-PPO complex (only residues located within 6 Å of ligand were calculated)

group of AFM was moved to position-4 of RH. This structural modification did not change significantly the electrostatic and *van der Waals* interaction energies. However, due to the position of CF_3 is changed from position-3 to position-4, RH has to take different conformation from AFM to optimize its interaction with the protein. Therefore, the entropy contribution to the binding free energy of RH became significantly unfavorable, which accounts for the binding affinity decrease of RH. Interestingly, earlier QSAR study also indicated that

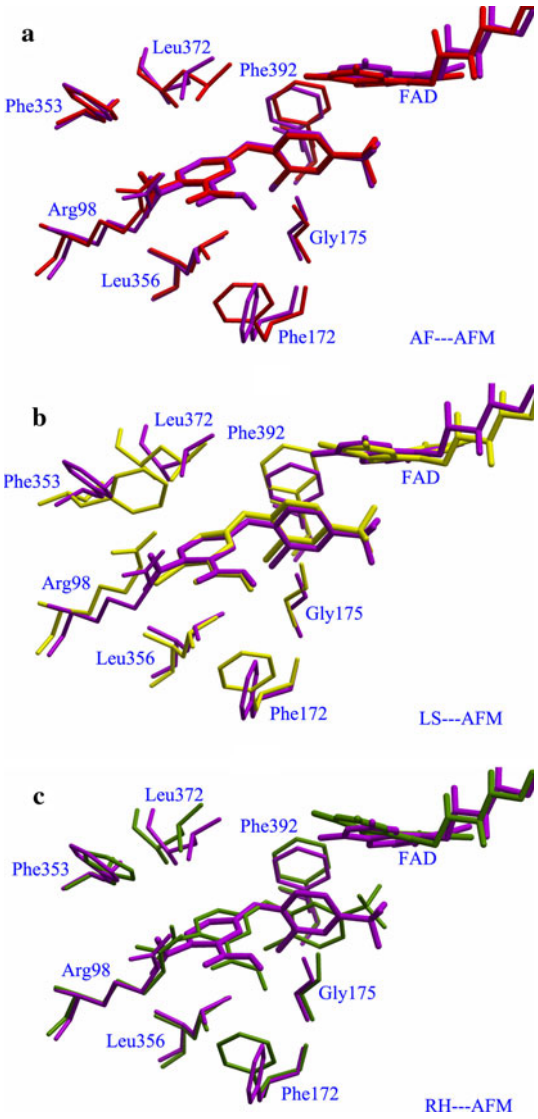

Fig. 5 Superimposition of the average complexes structures from the last 1 ns of the MD trajectories. **a** Superimposition between AF-PPO complex and AFM-PPO complex, **b** Superimposition between LS-PPO complex and AFM-PPO complexes, and **c** Superimposition between RH-PPO and AFM-PPO complex

substituents at position-4 was unfavorable to the PPO-inhibiting activity [60].

The above analysis showed that hydrophobic interaction is important for the potency of PPO inhibitors. To better understand the contribution of hydrogen-bond interactions, we calculated quantitatively the hydrogen bond energies of four inhibitors as summarized in Table 3. Obviously, LS has the lowest hydrogen bond energy, which inferred that the NO_2 group is vital, the lost of which can also weaken the hydrogen bond between Arg98 and the oxygen atom on position-9. It is probably the reason that this type of compounds were called nitrophenyl-ether herbicide earlier [60]. However, it is well known that the ligand-solvent hydrogen bond energy, as a main part of desolvation penalty can cancel the effect of the ligand-receptor hydrogen bond energy. So in order to know which one will contribute more, we have compared the difference between them, which have been put in the supplementary material (Table S1). From the results of the comparison, the effect of ligand-solvent hydrogen bonds could only partly cancel the hydrogen bonds effect of the ligand-receptor interaction, and this will not influence the conclusion that ligand-receptor hydrogen bond energy plays key role on the binding affinity.

Conclusions

In summary, molecular dynamics simulations, approximate free energy calculations and hydrogen bond energy calculations were integrated together to uncover the structure–activity relationships of four diphenyl-ether inhibitors of PPO. According to the established computational models and the results of approximate free energy calculation, we can conclude that: (1) position-1,-2,-3,-4, and -5 should be substituted with hydrophobic groups due to the hydrophobic property of the binding pocket. (2) Position-4 should not be substituted by large groups in order to obtain

Table 3 Comparision of hydrogen bond energies

Ligand	Acceptor	Donor (H)	%[a]	Maximum distance[b]	Minimum distance	Average distance	HBE[c]
AF	AF: O[d]	Arg98: NE (H)	64.45	6.15	1.66	2.62 (0.03)[e]	−3.49 (0.11)
AFM	AFM: O	Arg98: NE (H)	71.20	4.67	1.69	2.42 (0.01)	−3.46 (0.09)
LS	LS: O	Arg98: NE (H)	58.60	4.63	1.64	2.64 (0.02)	−2.43 (0.09)
RH	RH: O	Arg98: NE (H)	64.10	3.97	1.65	2.40 (0.01)	−3.46 (0.10)

[a] Occupancy of hydrogen bonds (The occupancy > 50% were listed)

[b] Hydrogen bond distance (Å)

[c] Hydrogen bond energy (kcal/mol), calculated according to $\mathrm{HBE}(r) \approx 5\varepsilon r_{eqm}^{12}/r^{12} - 6\varepsilon r_{eqm}^{10}/r^{10}$, the parameters: $r_{\mathrm{eqm(H\ldots O)}} = 1.90$ Å, $\varepsilon_{\mathrm{(H\ldots O)}} = 8.4$ kcal/mol.[56] We calculated the HBE of every snapshot in the last 1 ns and then took the average value

[d] Oxygen atom is the carbonyl oxygen on position-9

[e] The values in parentheses are standard error (SE)

better match with the surrounding residues. (3) Position-8 and -9 should be substituted by electronegative groups to increase the electrostatic interaction with Arg98. (4) Position-8 can also be substituted by small hydrophobic and electronegative groups (e.g. halogen) due to the entropy compensation mechanism. (5) Position-9 should be occupied by bulky groups with hydrogen bond acceptor atoms to form *van der Waals* interaction and hydrogen-bond interactions with the surrounding residues. These insights from computational simulations will be helpful for the understanding of PPO-inhibitor interaction mechanism, but also benefit to the future rational design of novel PPO inhibitors with improved potency.

Acknowledgments The research was supported in part by the National Basic Research Program of China (No. 2010CB126103), the NSFC (No. 20925206 and 20932005) and the PCSIRT (No. IRT0953).

References

1. Porra RJ, Falk JE (1964) Biochem J 90:69
2. Gerald SM (1966) Bot Rev 32:56
3. Poulson R, Polglase WJ (1975) J Biol Chem 250(4):1269
4. Ferreira GC, Andrew TL, Karr SW, Dailey HA (1988) J Biol Chem 263(8):3835
5. Lermontova I, Kruse E, Mock HP, Grimm B (1997) Proc Natl Acad Sci U S A 94(16):8895
6. Jacobs JM, Jacobs NJ (1984) Arch Biochem Biophys 229(1):312
7. Poulson R (1976) J Biol Chem 251(12):3730
8. Beale SI (1999) Photosynth Res 60(1):43
9. Duke SO, Lydon J, Becerril JM, Sherman TD, Lehnen LP, Matsumoto H (1991) Weed Sci 39(3):456
10. Duke SO, Nandihalli UB, Lee HJ, Duke MV (1994) ACS Symp Ser 559:191
11. Arnould S, Camadro JM (1998) Proc Natl Acad Sci U S A 95(18):10553
12. Matringe M, Camadro JM, Labbe P, Scalla R (1989) Biochem J 260:231
13. Meazza G, Bettarini F, La Porta P, Piccardi P, Signorini E, Portoso D, Fornara L (2004) Pest Manag Sci 60(12):1178
14. Hess FD (2000) Weed Sci 48(2):160
15. Scalla R, Matringe M (1994) Rev Weed Sci 6:103
16. Jacobs JM, Jacobs NJ, Sherman TD, Duke SO (1991) Plant Physiol 97(1):197
17. Wettlaufer SH, Alscher R, Strick C (1985) Plant Physiol 78(2):215
18. Duke SO, Rebeiz CA (1994) ACS Symp Ser 559:71
19. Fingar VH, Wieman TJ, McMahon KS, Haydon PS, Halling BP, Yuhas DA, Winkelman JW (1997) Cancer Res 57(20):4551
20. Volker A, Burkhard G (2005) US Patent 20050049228
21. Boehncke WH, Konig K, Kaufmann R, Scheffold W, Prummer O, Sterry W (1994) Arch Dermatol Res 286(6):300
22. Cruess AF, Zlateva G, Pleil AM, Wirostko B (2009) Acta Ophthalmol 87(2):118
23. Robertson CA, Evans DH, Abrahamse H (2009) J Photochem Photobiol B 96(1):1
24. Moghissi K, Dixon K, Stringer M, Thorpe JA (2009) Photodiagnosis Photodyn Ther 6(3–4):159
25. Kennedy JC, Pottier RH, Pross DC (1990) J Photochem Photobiol B 6(1–2):143
26. Halling BP, Yuhas DA, Fingar VF, Winkelmann JW (1994) American Chemical Society, Washington, p 280
27. Shepherd M, Dailey HA (2005) Anal Biochem 344(1):115
28. Maneli MH, Corrigall AV, Klump HH, Davids LM, Kirsch RE, Meissner PN (2003) Biochim Biophys Acta 1650(1–2):10
29. Nandihalli UB, Duke MV, Duke SO (1992) Pestic Biochem Physiol 43(3):193
30. Lee HJ, Duke MV, Birk JH, Yamamoto M, Duke SO (1995) J Agric Food Chem 43(10):2722
31. Sumida M, Niwata S, Fukami H, Tanaka T, Wakabayashi K, Boeger P (1995) J Agric Food Chem 43(7):1929
32. Koch M, Breithaupt C, Kiefersauer R, Freigang J, Huber R, Messerschmidt A (2004) EMBO J 23(8):1720
33. Corradi HR, Corrigall AV, Boix E, Mohan CG, Sturrock ED, Meissner PN, Acharya KR (2006) J Biol Chem 281(50):38625
34. Qin X, Sun L, Wen X, Yang X, Tan Y, Jin H, Cao Q, Zhou W, Xi Z, Shen Y (2010) J Struct Biol 170(1):76
35. Dailey TA, Dailey HA (1996) Protein Sci 5(1):98
36. Puy H, Robreau AM, Rosipal R, Nordmann Y, Deybach JC (1996) Biochem Biophys Res Commun 226(1):226
37. Camadro JM, Matringe M, Scalla R, Labbe P (1991) Biochem J 277(Pt 1):17
38. Frisch MJ, Trucks GW, Schlegel HB, Scuseria GE, Robb MA, Cheeseman JR, Montgomery JA, Vreven T, Kudin KN, Burant JC, Millam JM, Iyengar SS, Tomasi J, Barone V, Mennucci B, Cossi M, Scalmani G, Rega N, Petersson GA, Nakatsuji H, Hada M, Ehara M, Toyota K, Fukuda R, Hasegawa J, Ishida M, Nakajima T, Honda Y, Kitao O, Nakai H, Klene M, Li X, Knox JE, Hratchian HP, Cross JB, Bakken V, Adamo C, Jaramillo J, Gomperts R, Stratmann RE, Yazyev O, Austin AJ, Cammi R, Pomelli C, Ochterski JW, Ayala PY, Morokuma K, Voth GA, Salvador P, Dannenberg JJ, Zakrzewski VG, Dapprich S, Daniels AD, Strain MC, Farkas O, Malick DK, Rabuck AD, Raghavachari K, Foresman JB, Ortiz JV, Cui Q, Baboul AG, Clifford S, Cioslowski J, Stefanov BB, Liu G, Liashenko A, Piskorz P, Komaromi I, Martin RL, Fox DJ, Keith T, Al-Laham MA, Peng CY, Nanayakkara A, Challacombe M, Gill PMW, Johnson B, Chen W, Wong MW, Gonzalez C, Pople JA (2003) Gaussian 03, revision B-03. Gaussian Inc., Pittsburgh
39. Singh UC, Kollman PA (1984) J Comput Chem 5(2):129
40. Besler BH, Merz KM, Kollman PA (1990) J Comput Chem 11(4):431
41. Case DA, Darden TA, Cheatham TE, Simmerling CL, Wang J, Duke RE, Luo R, Merz KM, Wang B, Pearlman DA, Crowley M, Brozell S, Tsui V, Gohlke H, Mongan J, Hornak V, Cui G, Beroza P, Schafmeister C, Caldwell JW, Ross WS, Kollman PA (2004) AMBER 8. University of California, San Francisco
42. Sybyl7.1. Tripos Inc., St. Louis
43. Wang J, Cieplak P, Kollman PA (2000) J Comput Chem 21(12):1049
44. Wang J, Wolf RM, Caldwell JW, Kollman PA, Case DA (2004) J Comput Chem 25(9):1157
45. Jorgensen WL, Chandrasekhar J, Madura JD, Impey RW, Klein ML (1983) J Chem Phys 79(2):926
46. Darden T, York D, Pedersen L (1993) J Chem Phys 98(12):10089
47. Essmann U, Perera L, Berkowitz ML (1995) J Chem Phys 103(19):8577
48. Ryckaert JP, Ciccotti G, Berendsen HJC (1977) J Comput Phys 23(3):327
49. Kollman PA, Massova I, Reyes C, Kuhn B, Huo S, Chong L, Lee M, Lee T, Duan Y, Wang W, Donini O, Cieplak P, Srinivasan J, Case DA, Cheatham TE 3rd (2000) Acc Chem Res 33(12):889
50. Gilson MK, Sharp KA, Honig BH (1987) J Comput Chem 9(4):327

51. Sitkoff D, Sharp KA, Honig B (1994) J Phys Chem 98(7):1978
52. Case DA, Cheatham TE 3rd, Darden T, Gohlke H, Luo R, Merz KM Jr, Onufriev A, Simmerling C, Wang B, Woods RJ (2005) J Comput Chem 26(16):1668
53. Hao G-F, Yang G-F (2010) PLoS ONE 5(5):e10742
54. Hao GF, Yang GF, Zhan CG (2010) J Phys Chem B 114(29):9663
55. Morris GM, Goodsell DS, Halliday RS, Huey R, Hart WE, Belew RK, Olson AJ (1998) J Comput Chem 19(14):1639
56. Hao GF, Zhu XL, Ji FQ, Zhang L, Yang GF, Zhan CG (2009) J Phys Chem B 113(14):4865
57. InsightII. Molecular Simulation, Inc., San Diego
58. Moritsugu K, Njunda BM, Smith JC (2010) J Phys Chem B 114(3):1479
59. Durst GL (1998) Quant Struct-Act Relat 17:419
60. Davan FE, Allen SN (2000) Pest Manag Sci 56(8):717